



# Fractal Attractor of the Deep Convection Cycle in the Northwest Mediterranean Sea

Douglas Keller Jr.<sup>1</sup>

<sup>1</sup>LMD/IPSL, École Polytechnique, Institut Polytechnique de Paris, ENS, PSL Research University, Sorbonne Université, CNRS, Palaiseau, France

**Correspondence:** Douglas Keller Jr. (dg.kllr.jr@gmail.com)

**Abstract.** Deep convection in the Gulf of Lion is an important ocean mixing process in the western Mediterranean Sea caused by large cooling fluxes at the sea surface. It aids the Mediterranean thermohaline circulation, and promotes phytoplankton blooming. This work investigates the three different periods of the process: preconditioning, deep convecting, and restratification, through the lens of fractal attractor analysis with the local correlation dimension. From the analysis it was determined that preconditioning period is most predictable period, with a local correlation dimension of 10 to 30, followed by the deep convecting period, with a local correlation dimension of 30 to 45. However, the deep convecting period can also exhibit random process like behavior with local correlation dimensions growing exceedingly high in April and May. The least predictable period was the restratification period, with typical local correlation dimensions of 50 to 80 near the end of restratification.

## 1 Introduction

Geophysical flows are perhaps the most classical example of chaotic behavior. This result is well captured and demonstrated by the work of Lorenz (Lorenz, 1963). In the ocean, typically this behavior is captured through the intrinsic ocean variability computed through ensemble modelling (Sérazin et al., 2015), where it strongly influences the smaller spatial scales (length scales less than 6 °) and time scales (less than 18 months) but also the larger scales (Sérazin et al., 2015; Grégorio et al., 2015).

Open ocean deep convection occurs semi-frequently in the Gulf of Lion, in the northwest Mediterranean Sea (Somot et al., 2016). In this region, the process is driven by strong air-sea heat fluxes that cool the water surface over time until the vertical density gradient is eroded and it can convect. The Mistral and Tramontane winds, along with seasonal changes in the atmosphere over the gulf, create these fluxes (Keller Jr. et al., 2022; Keller et al., 2024). The process itself occurs primarily in three periods: the preconditioning period, deep convecting period, and restratification period (Marshall and Schott, 1999; Group, 1998). The preconditioning period starts near the end of summer and progresses with the gentle deepening of the mixed layer until roughly February, where if enough cooling at the sea surface has occurred, the deep convection period is triggered. Deep convection can last for a few days to a few weeks, before horizontal gradient of less dense fluids surrounding the deep convection patch overcome the vertical mixing and restratify the vertical column (Madec et al., 1991). This last step is called the restratification period, and lasts until the beginning of summer.



Deep convection in the Gulf of Lion generates the Western Mediterranean Deep Water (WMDW) from its intense vertical mixing of cooled Atlantic Water (AW) and Eastern Intermediate Water (EIW), which aids the general thermohaline circulation of the Mediterranean Sea (Robinson et al., 2001). After its formation, the WMDW spreads out along the bottom of the western Mediterranean Sea basin (Group, 1970), flowing towards the Balearic Sea (Send and Testor, 2017), to south to the southern Algerian Basin within eddies (Beuvier et al., 2012; Testor and Gascard, 2003), and out the Atlantic Ocean through the Strait of Gibraltar. The vertical mixing also promotes oxygen and nutrient distribution along the vertical column, resulting in large phytoplankton blooms proceeding deep convection events (Coppola et al., 2017; Severin et al., 2017). As a consequence of the process's impact on other major phenomena, much effort has been devoted to understanding the deep convection process, and in particular the deep convection period of the three aforementioned periods.

Deep convection in the Gulf of Lion has been studied through the lens of chaotic behavior before and has shown to be influenced by the intrinsic variability of the ocean, which contributes around 15 to 30% of the total temporal variability, depending on the system parameter (Waldman et al., 2018). For example, the resulting dense water formation of WMDW is known to be significantly affected by the initial conditions when modelled (Léger et al., 2016) and shows considerable spread in post deep convection attributes. Other studies have noted the significant spread of the deep convection mixed layer depth with ensemble modelling, particularly for the winter of 2012/2013 (Waldman et al., 2017b, a). However, these works focus mainly on the deep convection period in particular, and less so on the other two periods. The focus is kept on the deep convection period due to previously mentioned motivation and because the convection itself is typically the most difficult part of the process to recreate via modelling. Therefore, the other two periods haven't had as much attention devoted to them.

This paper further dives into the chaotic nature of deep convection in the Gulf of Lion, but includes investigating the pre-conditioning and restratification periods. The method used here doesn't require ensemble modelling and perhaps more directly measures the chaotic behavior of the system at hand. The local dimensionality of the deep convection system, used in this work, is computed from a high spatial resolution reanalysis that covers from 1987 to 2022 (Escudier et al., 2021), which can be used to describe the chaotic variability, therefore the predictability, of each system state. The method does so by measuring the fractal dimension of the system's dynamic, fractal attractor for each time step (Lucarini et al., 2012; Faranda et al., 2017). By using this technique, we can determine the predictability of each time step of deep convection in the Gulf of Lion, and describe the resulting predictability of the three open ocean convection periods. In the methodology section that follows (Sec. 2), the local correlation dimension is described (the metric of local dimensionality) and the steps taken to revise the reanalysis dataset of the Gulf of Lion to be more representative of the mixed layer depth (MLD) found in other studies (e.g. in (Somot et al., 2016)). This is followed by the results and discussion sections (Sec. 3 and 4), where the calculated local dimensions are presented and the predictability of the three different deep convection periods are discussed, respectively. Concluding remarks follow in Sec. 5.



## 55 2 Methodology and Data

### 2.1 Local Correlation Dimension and Local Dimensionality

A method to understand the fractal attractor of a system from observations is to determine its local correlation dimension (also called pointwise dimension),  $d$ , through Extreme Value Theory (EVT) (Lucarini et al., 2012; Faranda et al., 2017).  $d$  is a flavor of the fractal dimension measuring techniques (Grassberger, 1983; Grassberger and Procaccia, 1983; Lopes and Betrouni, 2009; Strogatz, 2014) and here it effectively represents the local density of the system's states on its attractor (the recurrence of the system to that location). It measures the number of dimensions needed to describe the current state and implies the number of next states the system could evolve into ( $0 < d < \infty$ ), which effectively defines each state's predictability (Aurell et al., 1997; Boffetta et al., 1998). It can be computed by first determining the natural log of the distances between a particular system state (the first case observable in Lucarini et al. (2012)),  $\xi$ , and all other states,  $\mathbf{x}(t)$  (therefore  $\xi = \mathbf{x}(t_i)$ ):

$$65 \quad g_1 = -\ln(\text{dist}(\xi, \mathbf{x}(t))) \quad (1)$$

Then take an arbitrary threshold,  $T$ , to find the set of distances,  $z$ , that exceed this threshold (i.e.  $z = g_1 - T$ ). If  $T$  is sufficiently large (e.g. the 98th percentile of  $g_1$ ) and  $z$  primarily captures the extreme values of  $g_1$ , then the distribution of  $z$  follows that of the Generalized Pareto Distribution (GPD). Following Lucarini et al. (2012) and Faranda et al. (2017),  $d$  is the reciprocal of the mean value of  $z$ 's distribution. This means we have an estimation of the system's attractor's local correlation dimension for each provided system state, and therefore time step. Hereafter,  $d$  will be referred to as the local dimensionality of the given system state, which is consistent with other works using this method (e.g. Faranda et al. (2017)).

This methodology should be insensitive to both the choice of distance function,  $\text{dist}$ , and threshold,  $T$ . However, in application, both can have an impact on the final results (Faranda et al., 2017). In this study, the Euclidean distance is used as the distance function and the 98th percentile of  $g_1$  is taken as the threshold.

### 75 2.2 System State Variable: Mixed Layer Depth

For this study, the MLD will be taken as the representative system state of deep convection in the Gulf of Lion. This metric directly measures deep convection and conveniently captures the state of the temperature, salinity, and dynamics of the ocean. In particular, the MLD used is from the high resolution reanalysis of the Mediterranean Sea performed by the Centro Euro-Mediterraneo sui Cambiamenti Climatici (CMCC) (Escudier et al., 2021) with the Nucleus for European Modelling of the Ocean model (NEMO; <https://www.nemo-ocean.eu>; last accessed Apr. 23th, 2025) (Madec and the NEMO team, 2008). The reanalysis covers the years of 1987 to 2022 with a daily temporal resolution. It has a horizontal resolution of about 4 to 5 km ( $1/24^\circ$ ), with 141 unevenly spaced, vertical levels. It was accessed via the Copernicus Marine Service Data Store (CMEMS) ([https://doi.org/10.25423/CMCC/MEDSEA\\_MULTIYEAR\\_PHY\\_006\\_004\\_E3R1](https://doi.org/10.25423/CMCC/MEDSEA_MULTIYEAR_PHY_006_004_E3R1); last accessed Feb. 10th, 2025) and is the highest resolution reanalysis of the Mediterranean Sea available on CMEMS. For this work, only the values within the bounds

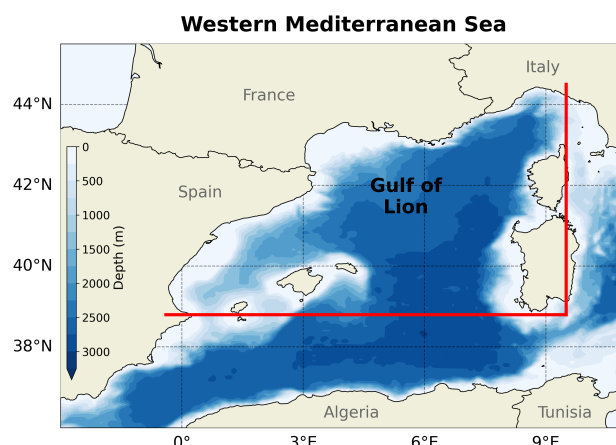


**Figure 1.** Study area with bathymetry: the Gulf of Lion in the northwestern Mediterranean Sea. The red lines mark the boundary of the area of interest (the eastern coast or  $-0.4$  to  $9.5$  °E and  $38.8$  °N to the northern coast or  $44.5$  °N).

85 of  $-0.4$  °E (the coast to the east) to  $9.5$  °E and  $38.8$  to  $44.5$  °N (the coast to the north) will be considered, as this area wholly captures the northwestern Mediterranean Sea and the Gulf of Lion within it (this area is shown in Fig. 1).

### 2.3 Argo Mixed Layer Depths

To cross check the validity of the reanalysis MLD, MLD calculations from Argo float profiles are used. The MLD calculations were performed by Holte et al. (2017) and provided at <https://mixedlayer.ucsd.edu>; last accessed: 22 February 2023). 17935  
90 MLD calculation points were used from this dataset, which covers this dataset's entire temporal range for the MLD spatial domain in Fig. 1. The MLD was determined via a density based algorithm (Holte and Talley, 2009) (also see <http://mixedlayer.ucsd.edu> for more details; last accessed: 22 February 2023). The algorithm they use is fairly in-depth and is only briefly presented here from their work: “the algorithm models the profile’s general shape, calculates a suite of possible MLD values, and then looks for groupings and patterns within the possible MLDs to select the final MLD estimate for each profile.”(Holte  
95 and Talley, 2009)

### 2.4 Modified Mixed Layer Depths

When comparing the Argo determined MLDs and reanalysis MLDs, the reanalysis seemingly overestimates the occurrence of deep convection in the Gulf of Lion (see 2 a)). The MLD maxima of the Argo data tends to remain less than 500 m for most years of its availability. Conversely, nearly all years of the reanalysis show MLD maxima below 1000 m. As the methodology  
100 to determine  $d$  is based on EVT, this over representation of deep convection can misrepresent the local dimensionality, as more system states will appear in the vicinity of true deep convection states than in observations. To make the MLD more representable of the actual system, misrepresentative states need to be removed.





**Table 1.** Fractions (percentages) of deep convection (DC) and non deep convection (NDC) years in varying literature used to revise the mixed layer depth dataset from the reanalysis (Escudier et al., 2021).

	Escudier et al. 2021 <sup>†</sup>	Somot et al. 2016	Margirier et al. 2020	Holte et al. 2017*	Escudier et al. 2021 Rev. <sup>‡</sup>
Years					
DC	34/36 (94.4%)	16/31 (51.6%)	5/11 (45.5%)	3/17 (17.6%)	16/36 (44.4%)
NDC	2/36 (5.6%)	15/31 (48.4%)	6/11 (54.5%)	14/17 (82.4%)	20/36 (55.6%)

<sup>†</sup>Original CMCC reanalysis mixed layer depth dataset. \*Argo mixed layer depth dataset. <sup>‡</sup>Revised reanalysis mixed layer depth dataset used for the dynamical analysis.

To keep the proper MLD states, we need information on deep convection before 2005, as this is the earliest data available from Argo profiles in the region. We also need more information for the year of 2015, as there is a gap in the Argo data there as well. The compilation of modelling and observation results from 1982 to 2013 in Somot et al. (2016) covers the first requirement and compiled observations in Margirier et al. (2020) covers the second requirement. In Fig. 2, the deep convection years (here taken as years with a maximum MLD below 1000 m in the region during the winter and spring) are marked with filled dots (red for the reanalysis, black for the Argo data, blue for the information from Somot et al. (2016), and green for the information from Margirier et al. (2020); empty dots denote non-convecting years). The years retained as deep convecting for a modified MLD reanalysis dataset are marked by the red, filled triangles (red empty "x"'s mark when the year was removed).

The following years had the reanalysis MLD states removed when the maximum MLD reached below 250 m and occurred between Oct. 1st of the previous year and June 1st of the current year: 1988, 1989, 1993, 1994, 1995, 1996, 1997, 1998, 2001, 2002, 2004, 2007, 2008, 2014, 2015, 2016, 2017, 2019, 2021. Comparatively, the original reanalysis MLD dataset had 94.4% of the years as deep convecting (see Tab. 1). The revised set has 44.4% of the years as deep convecting, which is more inline with both Somot et al. (2016) and Margirier et al. (2020) (51.6% and 45.4%, respectively; again refer to Tab. 1). The Argo MLD alone appears to under represent deep convection at 17.6%, but this is likely due to Somot et al. (2016) and Margirier et al. (2020) using more a complete set of observations (e.g. the Gulf of Lion mooring).

Figure 3 shows the resulting difference between the distributions of  $d$  for the original reanalysis MLD dataset,  $d_o$ , and the revised set,  $d_r$ , in a) and b). Subplot a) shows the density distribution of  $d$  for both sets, while the b) shows the cumulative density function of the % relative difference, as describe by:

$$\text{Relative Difference } (t) = \frac{|d_r(t) - d_o(t)|}{d_o(t)} \cdot 100 \quad (2)$$

From Fig. 3 b), we can see that  $\sim 90\%$  of  $d_r$  differ by 10% or less from their original values and 99% of them are under 25% different. Combined, with nearly identical distributions as seen in a), the revised MLD set is more representative of reality

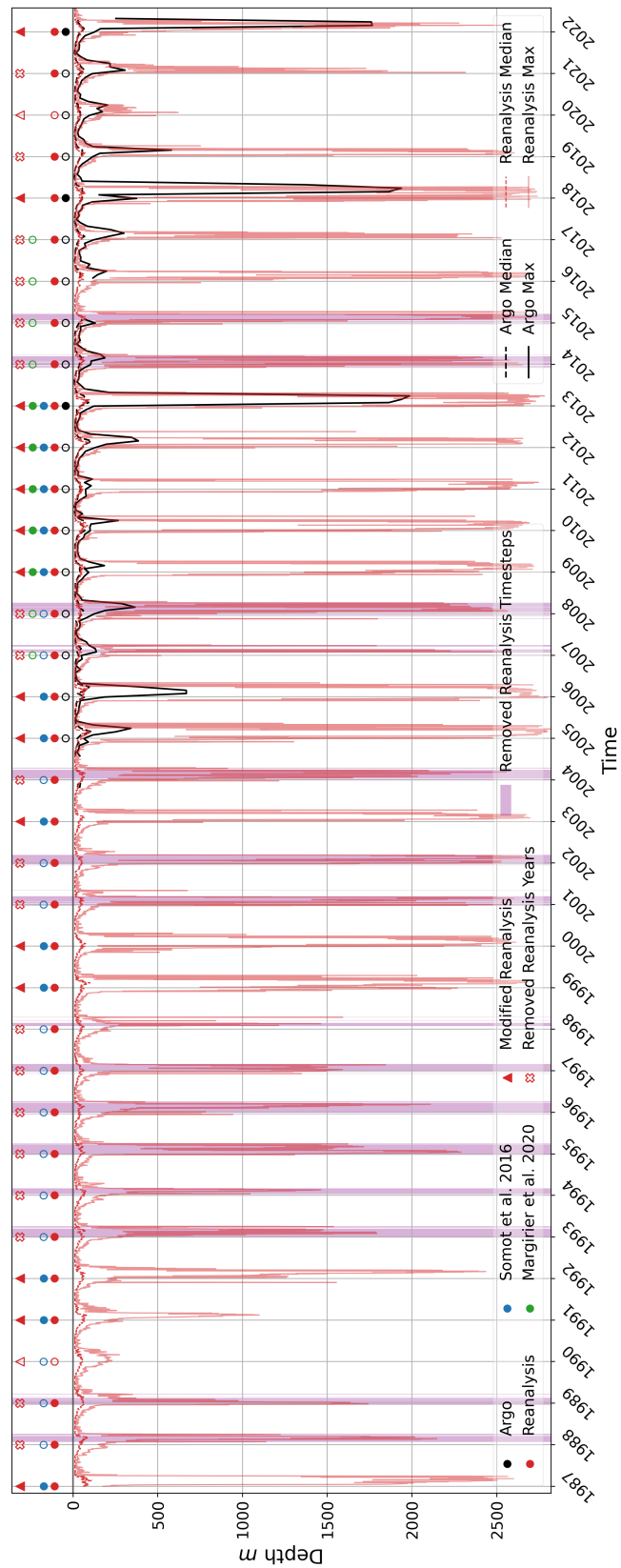


**Figure 2.** Mixed layer depth time series for the reanalysis and Argo observations with the occurrence of deep convection (as determined by a maximum MLD below 1000 m) from the reanalysis (red markers and lines), Argo observations (black markers and lines), Somot et al. (2016) (blue markers), and Marginier et al. (2020) (green markers). Filled dots mark deep convection years, unfilled dots mark non-deep convection years, and the filled triangles mark the years kept for the modified reanalysis MLD dataset. Empty red "x"s denote removed years, with the purple shading more explicitly showing the time steps removed. As the Argo MLDs were originally derived from profiles, the monthly maximum and median were taken for all values within the study area (Fig. 1).

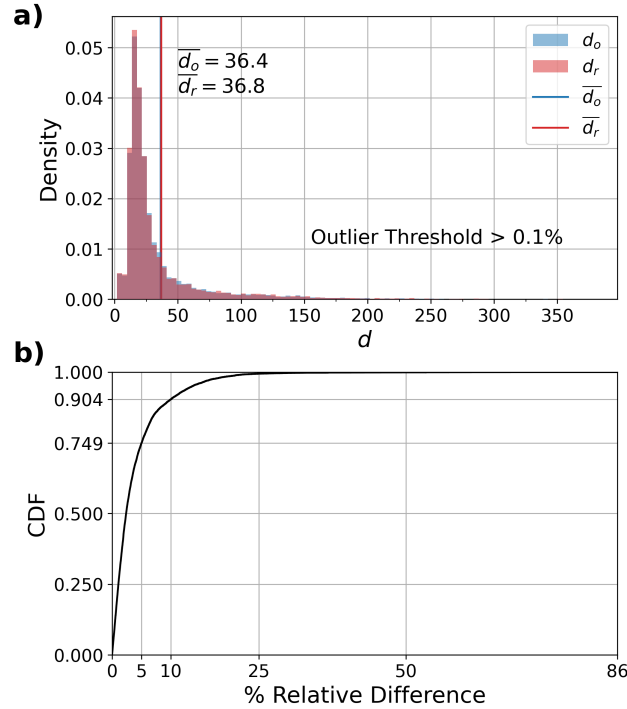


**Figure 3.** Differences in the distribution of local dimensionality between the original and revised dataset from the reanalysis (Escudier et al., 2021).  $d_o$  stands for the  $d$  calculated from the original reanalysis MLD set and  $d_r$  from the revised set. a) shows the density distributions of  $d_o$  and  $d_r$ . Outliers, determined as bins with counts less than 0.1% of the population of either  $d$  are not displayed. The overbarred variables are the average values. b) shows the cumulative density function of the % relative differences (Eq. 2) between  $d_o$  and  $d_r$  (same time steps are compared). Note that the CDF(25) equals 0.994.

while not significantly changing the results of the analysis. *N.B.: for the remaining sections of this work, unless otherwise mentioned,  $d$  will refer to  $d_r$ .*

### 3 Results

The resulting system trajectories of the local dimensionality of the MLD's fractal attractor are shown in Fig. 4.  $d$  varies significantly throughout the years at different depths, but there is a clear annual cycle. The months with the larger local dimensionality are found either during the late spring and summer months (ordinal days  $\sim 150$  to  $\sim 250$ ) or during deep convection (ordinal days  $\sim 0$  to  $\sim 100$ ). Conversely, during the months of September through January (ordinal days from  $\sim 250$  to  $\sim 365/366/0$ ), the local dimensionality is quite low. These results suggest that the preconditioning period, when the MLD is deepening, is the most predictable period, requiring the least number of dimensions to describe. However, the summer months are the least predictable, despite the water column being the most stable (Margirier et al., 2020; Keller et al., 2024).

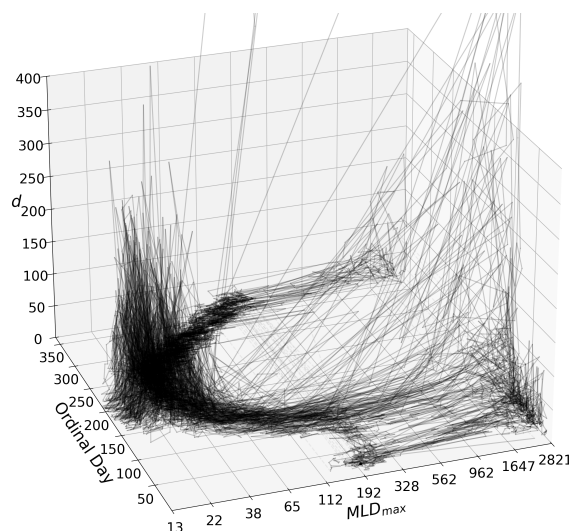


**Figure 4.**  $d$  trajectories of the modified MLD, marked by the maximum MLD on one axis (on a natural log axis), the day of the year on another axis, and the local dimensionality on the vertical. 28 values exceed 400 in the vertical (less than 0.2% of all  $d$ ) and are potentially random process like. This is also visualized later in Fig. 7 c). When the trajectories wrap around to the beginning of the year, the lines are lighter and dashed (the same is true for other large gaps in the trajectories from modifying the MLD dataset).

Initially, it appears that the local dimensionality is quite large during deep convection from Fig. 4. However, if we look at individual trajectories, such as those shown in Fig. 5, this isn't always true. Subplot c) shows for the exceptional case of the winter of 2012/2013, values sometimes exceed 400, agreeing with its exceptionalness. However, for winter of 2020/2021, shown in b),  $d$  during the deep convecting period remains quite low and less than that in the restratification period and summer. A non deep convecting winter, shown in a) (2019/2020), behaves similarly.

To get a clearer image of the seasonal distribution of  $d$  and see its behavior during the different deep convection cycle periods, Fig. 6 shows the monthly median, 25th, and 75th quantiles of both the  $d$  (subplot a)) and MLD maximum (subplot b)). From this figure, we can confirm that the summer months, particularly from May to September, show an enhanced local dimensionality. Additionally, we can confirm that the preconditioning period, from September to January is also the lowest, with the lowest spread in values. This is followed by the deep convecting and restratification periods, which have slightly higher values of  $d$  (comparing subplots a) and b) from March to May). This demonstrates that typically the local dimensionality during the deep convecting period is lower than the summer months, despite having some exceptional cases.

If we take Fig. 6 a step further, and look at the distribution of  $d$  with *depth and time*, then the local dimensionality of the deep convection cycle becomes more nuanced. When we now look at the median  $d$  during deep convection, focusing on Fig. 7 b) and c), we see that only part of the deep convection period is less predictable: the events with MLD maximum depths occurring partially in March, and during April and May, where  $d$  has some values exceeding 85. Deep convection with MLD maxima during December, January, and February have much lower values for  $d$ , around 30 to 45. These states are more comparable

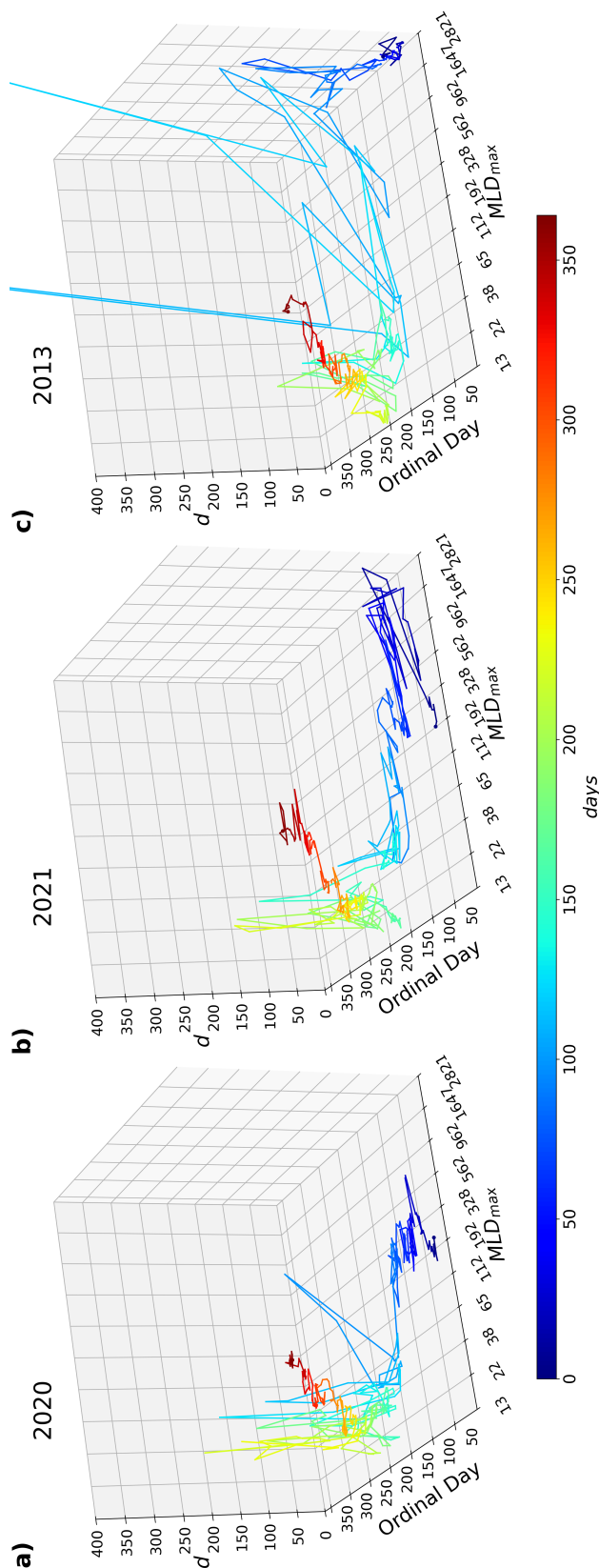


**Figure 5.** Selected yearlong trajectories from Fig. 4, from the initial day of the year til the end. The trajectory in a) shows the path for the year of 2020 (winter 2019/2020; a non deep convecting year) and the trajectory in b) shows the path for the year of 2021 (winter 2020/2021; a deep convecting year). c) shows the year of 2013 (winter of 2012/2013). The axes are the same as for Fig. 4, with the added visual aid of a color map for the time progression of the trajectories.

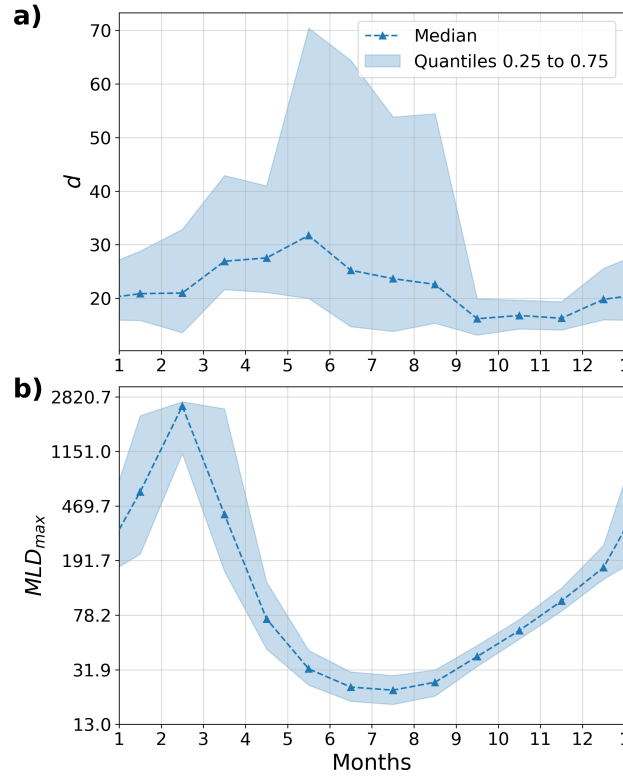


**Figure 6.** Seasonal distributions of  $d$ , a), and MLD maximum, b). The monthly medians are shown with the triangular markers and dashed lines, while the shading shows the region between the 25th and 75th percentiles. Note that the vertical axis for b) is natural logarithmic, again due to the logarithmic spacing of the vertical cells in the reanalysis model.

to the states with less deep MLD maxima found during the middle of the restratification period or when vertical mixing stays within the Eastern Intermediate Water layer. Notably, the regions of MLD maxima with large  $d$ , have values approaching 8000 (hence why they were separated into c)). This suggests that this region is more characterized as a random process, as random behavior tends to have values at or approaching infinity for  $d$ , as it takes an infinite number of dimensions to accurately describe (Victor, 1987; Argyris et al., 1998; Kondrashov et al., 2019) (but finite values of  $d$  for certain categories of random attractors exist (Debussche, 1997, 1998)). Fig. 7 a) and d) also show this region contains a low number of system states (seen in a) as the percentage of time steps present per bin) and low variability (seen as the difference between the 75th and 25th percentile of  $d$  per bin), lending support to the idea of these states are better characterized as a random process.

Returning back to the other system states, Fig. 7 b) confirms that during the months of September to the beginning of January, the local dimensionality is very low. Subplot d) reinforces this by showing that this region of phase space is also relatively low in variability. Subplot b) also confirms that  $d$  is larger during the summer months, with values around 50 to 80 (sometimes around 100), *albeit, when the system is restabilizing the MLD*. Instead, we can see the deeper MLDs leading into

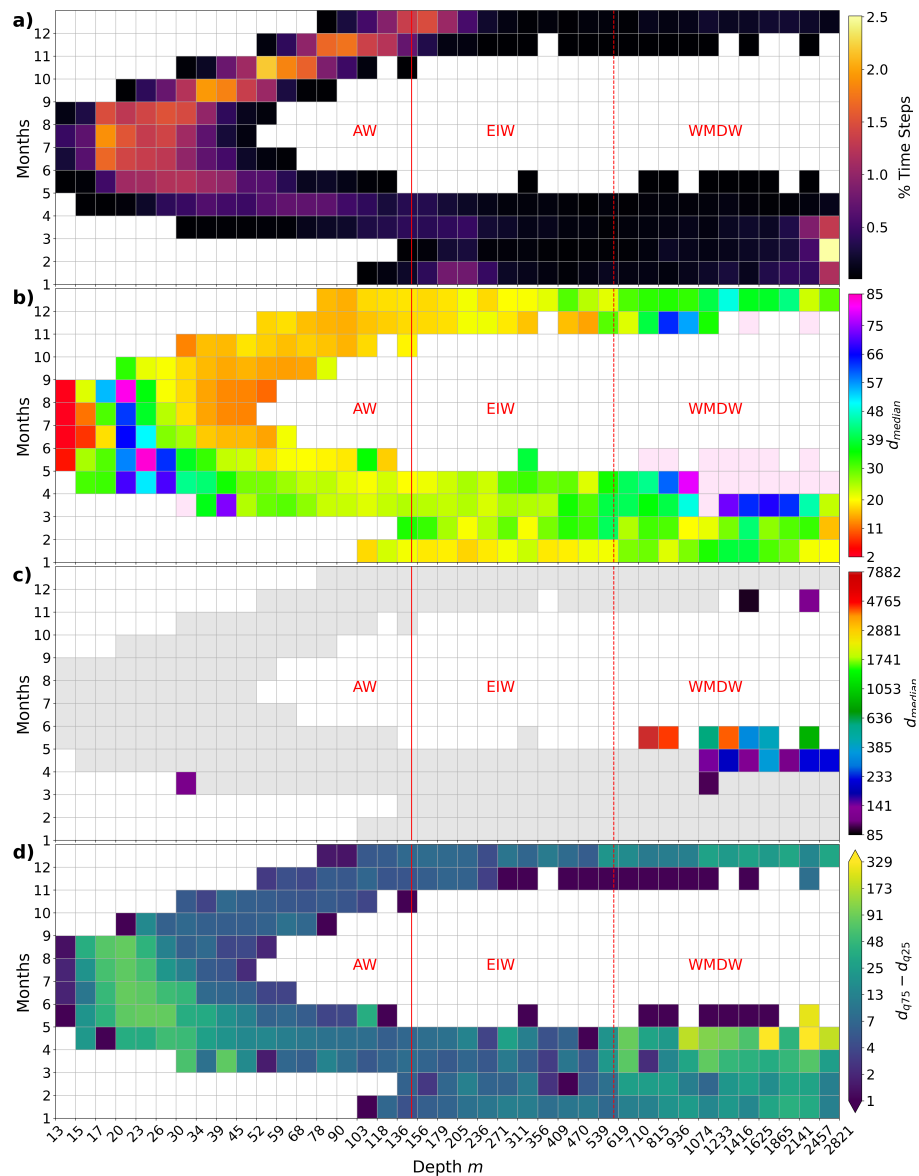


**Figure 7.** The seasonal and depth distribution of  $d$ , binned with respect to time and maximum MLD depth. Each bin is one month wide and has a depth side varying exponentially (increasing with depth). a) shows the percent occurrence of states within each bin. b) and c) both display the medians of  $d$ , with the b) showing 0 to 85 and c) showing from 85 to the maximum value. c)'s color bar is in log base 10, to more easily see the value separation versus natural log used for depth. d) shows the variability of  $d$  via the difference between each bin's 0.75 and 0.25 quantile. The Atlantic Water (AW), Eastern Intermediate Water (EIW), and Western Mediterranean Deep Water (WMDW) are shown with their general layer bounds: 0 to 150 m, 150 to 600 m, and 600 m and below, for each layer, respectively.





the preconditioning period, during the months of June, July, and August, have quite a low dimensionality, with values around the single digits to 20. We can also see the shallowest MLDs during these months have the lowest  $d$  over the whole distribution, approaching values of 2 (the fractal attractor's shape locally here is a plane), which isn't clearly visible in Fig. 4 or 6. Therefore, Fig. 7 b) clarifies that the summer months are the least predictable during the restratification period but are otherwise the most predictable system states.

## 4 Discussion

In geophysical fluids, the nonlinear, advective term in their mathematical description is the source of chaos in their systems (Lorenz, 1963). We can reason that the restratification period is the most consistently unpredictable part of the deep convection system, because the tracer field is dominated by horizontal gradients, as the less dense water surrounding the deep convection patch tries to reestablish a spatially stable density gradient. The baroclinic instability breaks apart the rim current (Madec et al., 1991), forming eddies that capture and maintain portions of the mixed patch to be transported elsewhere in the western Mediterranean basin (Bosse et al., 2016; Testor and Gascard, 2003). Conversely, the growth of the ocean MLD occurs non penetratively, even during deep convection, with the slow erosion of the density gradient without entraining plumes (Marshall and Schott, 1999). Therefore, the fluid itself and its tracers (salinity and temperature) at the interface with denser waters is relatively less turbulent. The findings here support the hypothesis of Waldman et al. (2018) that baroclinic instability generates much of the intrinsic variability in the deep convection system. In their work, they attributed the spatial intrinsic variability to the spatial variability of the baroclinic instability, as measured through a bathymetry aware Eady eddy theory (Blumsack and Gierasch, 1972; Isachsen, 2011, 2015). For this work, the method captures the spatial variability but only provides us with the instantaneous variability of the system in time, therefore the results here can only concur with Waldman et al. (2018)'s findings qualitatively.

A key point to note about using this methodology is that it measures the local dimensionality of a *particular system*. Therefore, while here it describes the chaotic behavior of the underlying fractal attractor of deep convection, it fundamentally relies on the particular model used to represent this phenomenon, which in this case is NEMO. NEMO has been used extensively to investigate deep convection in the Gulf of Lion (Waldman et al., 2018, 2017a; Lebeaupin Brossier et al., 2017; Houpert et al., 2016; Waldman et al., 2017b; L'Hévéder et al., 2012; Lebeaupin Brossier et al., 2012; Beuvier et al., 2012; Herrmann et al., 2010; Lebeaupin Brossier and Drobinski, 2009), and so the analysis here is relevant. However, NEMO employs a number of assumptions that could affect the transferability of this analysis. It employs the spherical Earth and thin shell approximation, neglects the cosine component of the Coriolis rotation vector, and assumes the turbulent closure, Boussinesq, hydrostatic, and incompressible fluid hypotheses. The last four assumptions could potentially alter the analysis presented here if they are relaxed or removed, as all four involve some level of nonlinearity. Additionally, the hydrostatic hypotheses has the consequence that the convective process in NEMO (and other hydrostatic models) is parameterized, and, depending on its implementation may or may not introduce more or less nonlinearity (as convection is inherently a nonlinear process). Therefore, using this anal-



195 ysis with an idealized, nonhydrostatic version of deep convection would be needed to determine if it is sensitive to convection  
being parameterized or not.

## 5 Conclusions

The results shown here present a general progression of the predictability of the deep convection system in the Gulf of Lion. Starting from the late the summer months, the system is relatively quite predictable, with a local dimension ranging from 10 to  
200 20. As the system enters the preconditioning period and the MLD deepens, the local dimension slowly grows, reaching 20 to 30 by the turn of the year. If deep convection occurs, the system sees an increase in its local dimension to around 30 to 45, if the system restratifies before March. Otherwise, the system appears to behave randomly with exceedingly large values. Once the system restratifies and the MLD decreases, the largest, non-random states are found during the end of the restratification period, with the local dimension ranging from 50 to 85. Counterintuitively, these large values are found squarely during the  
205 summer months. With that said, the system can also reach an effectively 2D state during the summer, if it becomes exceedingly stable.

From this analysis, the restratification period is consistently more chaotic and less predictable than the deep convection period, with some exceptions. As the restratification period sets up the conditions for the (potential) proceeding deep convection process, after a very predictable preconditioning period, better recreating and better understanding the restratification process  
210 may improve the reproducibility of deep convection in modelling efforts. This could be particularly important for long running simulations, with multiple restratification periods, and therefore, warrants further investigation.

*Data availability.* The Mediterranean Sea reanalysis performed by the Centro Euro-Mediterraneo sui Cambiamenti Climatici (CMCC) (Escudier et al., 2021) is available via the Copernicus Marine Service Data Store (CMEMS) at [https://doi.org/10.25423/CMCC/MEDSEA\\_MULTIYEAR\\_PHY\\_006\\_004\\_E3R1](https://doi.org/10.25423/CMCC/MEDSEA_MULTIYEAR_PHY_006_004_E3R1); last accessed Feb. 10th, 2025. The Argo mixed layer depth data is available at <https://mixedlayer.ucsd.edu>; last accessed: 22 February 2023 (Holte et al., 2017).  
215

*Author contributions.* Douglas Keller Jr. is the sole author and sole contributor.

*Competing interests.* The author declares no competing interests.

*Acknowledgements.* This work was supported by the Fond Ifker pour le climat managed by the Fondation de l'École Polytechnique.



## References

- Argyris, J., Andreadis, I., Pavlos, G., and Athanasiou, M.: The influence of noise on the correlation dimension of chaotic attractors, *Chaos, Solitons & Fractals*, 9, 343–361, [https://doi.org/10.1016/s0960-0779\(97\)00120-3](https://doi.org/10.1016/s0960-0779(97)00120-3), 1998.
- Aurell, E., Boffetta, G., Crisanti, A., Paladin, G., and Vulpiani, A.: Predictability in the large: an extension of the concept of Lyapunov exponent, *Journal of Physics A: Mathematical and General*, 30, 1–26, <https://doi.org/10.1088/0305-4470/30/1/003>, 1997.
- Beuvier, J., Béranger, K., Lebeaupin Brossier, C., Somot, S., Sevault, F., Drillet, Y., Bourdallé-Badie, R., Ferry, N., and Lyard, F.: Spreading of the Western Mediterranean Deep Water after winter 2005: Time scales and deep cyclone transport, *Journal of Geophysical Research: Oceans*, 117, <https://doi.org/10.1029/2011jc007679>, 2012.
- Blumsack, S. L. and Gierasch, P. J.: Mars: The Effects of Topography on Baroclinic Instability, *Journal of the Atmospheric Sciences*, 29, 1081–1089, [https://doi.org/10.1175/1520-0469\(1972\)029<1081:mteoto>2.0.co;2](https://doi.org/10.1175/1520-0469(1972)029<1081:mteoto>2.0.co;2), 1972.
- Boffetta, G., Giuliani, P., Paladin, G., and Vulpiani, A.: An Extension of the Lyapunov Analysis for the Predictability Problem, *Journal of the Atmospheric Sciences*, 55, 3409–3416, [https://doi.org/10.1175/1520-0469\(1998\)055<3409:aeotla>2.0.co;2](https://doi.org/10.1175/1520-0469(1998)055<3409:aeotla>2.0.co;2), 1998.
- Bosse, A., Testor, P., Houpert, L., Damien, P., Prieur, L., Hayes, D., Taillandier, V., Durrieu de Madron, X., d’Ortenzio, F., Coppola, L., Karstensen, J., and Mortier, L.: Scales and dynamics of Submesoscale Coherent Vortices formed by deep convection in the northwestern Mediterranean Sea, *Journal of Geophysical Research: Oceans*, 121, 7716–7742, <https://doi.org/10.1002/2016jc012144>, 2016.
- Coppola, L., Prieur, L., Taupier-Letage, I., Estournel, C., Testor, P., Lefevre, D., Belamari, S., LeReste, S., and Taillandier, V.: Observation of oxygen ventilation into deep waters through targeted deployment of multiple Argo-O<sub>2</sub> floats in the north-western Mediterranean Sea in 2013, *Journal of Geophysical Research: Oceans*, 122, 6325–6341, <https://doi.org/10.1002/2016jc012594>, 2017.
- Debussche, A.: On the finite dimensionality of random attractors I, *Stochastic Analysis and Applications*, 15, 473–491, <https://doi.org/10.1080/07362999708809490>, 1997.
- Debussche, A.: Hausdorff dimension of a random invariant set, *Journal de Mathématiques Pures et Appliquées*, 77, 967–988, [https://doi.org/10.1016/s0021-7824\(99\)80001-4](https://doi.org/10.1016/s0021-7824(99)80001-4), 1998.
- Escudier, R., Clementi, E., Cipollone, A., Pistoia, J., Drudi, M., Grandi, A., Lyubartsev, V., Lecci, R., Aydogdu, A., Delrosso, D., Omar, M., Masina, S., Coppini, G., and Pinardi, N.: A High Resolution Reanalysis for the Mediterranean Sea, *Frontiers in Earth Science*, 9, <https://doi.org/10.3389/feart.2021.702285>, 2021.
- Faranda, D., Messori, G., and Yiou, P.: Dynamical proxies of North Atlantic predictability and extremes, *Scientific Reports*, 7, <https://doi.org/10.1038/srep41278>, 2017.
- Grassberger, P.: Generalized dimensions of strange attractors, *Physics Letters A*, 97, 227–230, [https://doi.org/10.1016/0375-9601\(83\)90753-3](https://doi.org/10.1016/0375-9601(83)90753-3), 1983.
- Grassberger, P. and Procaccia, I.: Measuring the strangeness of strange attractors, *Physica D: Nonlinear Phenomena*, 9, 189–208, [https://doi.org/10.1016/0167-2789\(83\)90298-1](https://doi.org/10.1016/0167-2789(83)90298-1), 1983.
- Grégorio, S., Penduff, T., Sérazin, G., Molines, J.-M., Barnier, B., and Hirschi, J.: Intrinsic Variability of the Atlantic Meridional Overturning Circulation at Interannual-to-Multidecadal Time Scales, *Journal of Physical Oceanography*, 45, 1929–1946, <https://doi.org/10.1175/jpo-d-14-0163.1>, 2015.
- Group, M.: Observation of Formation of Deep Water in the Mediterranean Sea, 1969, *Nature*, 227, 1037–1040, <https://doi.org/10.1038/2271037a0>, 1970.



- 255 Group, T. L. S.: The Labrador Sea Deep Convection Experiment, *Bulletin of the American Meteorological Society*, 79, 2033–2058, [https://doi.org/10.1175/1520-0477\(1998\)079<2033:tlsdce>2.0.co;2](https://doi.org/10.1175/1520-0477(1998)079<2033:tlsdce>2.0.co;2), 1998.
- Herrmann, M., Sevault, F., Beuvier, J., and Somot, S.: What induced the exceptional 2005 convection event in the northwestern Mediterranean basin? Answers from a modeling study, *Journal of Geophysical Research: Oceans*, 115, <https://doi.org/10.1029/2010jc006162>, 2010.
- Holte, J. and Talley, L.: A New Algorithm for Finding Mixed Layer Depths with Applications to Argo Data and Subantarctic Mode Water Formation\*, *Journal of Atmospheric and Oceanic Technology*, 26, 1920–1939, <https://doi.org/10.1175/2009jtecho543.1>, 2009.
- 260 Holte, J., Talley, L. D., Gilson, J., and Roemmich, D.: An Argo mixed layer climatology and database, *Geophysical Research Letters*, 44, 5618–5626, <https://doi.org/10.1002/2017gl073426>, 2017.
- Houpert, L., Durieu de Madron, X., Testor, P., Bosse, A., D’Ortenzio, F., Bouin, M. N., Dausse, D., Le Goff, H., Kunesch, S., Labaste, M., Coppola, L., Mortier, L., and Raimbault, P.: Observations of open-ocean deep convection in the northwestern Mediterranean Sea: Seasonal and interannual variability of mixing and deep water masses for the 2007–2013 Period: DEEP CONVECTION OBS. NWMED 2007–2013, *Journal of Geophysical Research: Oceans*, 121, 8139–8171, <https://doi.org/10.1002/2016jc011857>, 2016.
- 265 Isachsen, P. E.: Baroclinic instability and eddy tracer transport across sloping bottom topography: How well does a modified Eady model do in primitive equation simulations?, *Ocean Modelling*, 39, 183–199, <https://doi.org/10.1016/j.ocemod.2010.09.007>, 2011.
- Isachsen, P. E.: Baroclinic instability and the mesoscale eddy field around the Lofoten Basin, *Journal of Geophysical Research: Oceans*, 120, 2884–2903, <https://doi.org/10.1002/2014jc010448>, 2015.
- 270 Keller, D., Givon, Y., Pennel, R., Raveh-Rubin, S., and Drobinski, P.: Untangling the Mistral and Seasonal Atmospheric Forcing Driving Deep Convection in the Gulf of Lion: 1993–2013, *Journal of Geophysical Research: Oceans*, 129, <https://doi.org/10.1029/2022jc019245>, 2024.
- Keller Jr., D., Givon, Y., Pennel, R., Raveh-Rubin, S., and Drobinski, P.: Untangling the mistral and seasonal atmospheric forcing driving deep convection in the Gulf of Lion: 2012–2013, *Ocean Science*, 18, 483–510, <https://doi.org/10.5194/os-18-483-2022>, 2022.
- 275 Kondrashov, A. V., Ustinov, A. B., Volobuev, E. S., Drozdovskii, A. V., and Kalinikos, B. A.: Investigation of noise influence on calculation of fractal dimension, *Journal of Physics: Conference Series*, 1400, 044 002, <https://doi.org/10.1088/1742-6596/1400/4/044002>, 2019.
- Lebeaupin Brossier, C. and Drobinski, P.: Numerical high-resolution air-sea coupling over the Gulf of Lions during two tramontane/mistral events, *Journal of Geophysical Research: Atmospheres*, 114, <https://doi.org/10.1029/2008jd011601>, 2009.
- 280 Lebeaupin Brossier, C., Béranger, K., and Drobinski, P.: Sensitivity of the northwestern Mediterranean Sea coastal and thermohaline circulations simulated by the 1/12°-resolution ocean model NEMO-MED12 to the spatial and temporal resolution of atmospheric forcing, *Ocean Modelling*, 43–44, 94–107, <https://doi.org/10.1016/j.ocemod.2011.12.007>, 2012.
- Lebeaupin Brossier, C., Léger, F., Giordani, H., Beuvier, J., Bouin, M., Ducrocq, V., and Fourrié, N.: Dense water formation in the northwestern Mediterranean area during HyMeX-SOP2 in 1/36° ocean simulations: Ocean-atmosphere coupling impact, *Journal of Geophysical Research: Oceans*, 122, 5749–5773, <https://doi.org/10.1002/2016jc012526>, 2017.
- 285 Léger, F., Lebeaupin Brossier, C., Giordani, H., Arsouze, T., Beuvier, J., Bouin, M., Bresson, É., Ducrocq, V., Fourrié, N., and Nuret, M.: Dense water formation in the north-western Mediterranean area during HyMeX-SOP2 in 1/36° ocean simulations: Sensitivity to initial conditions, *Journal of Geophysical Research: Oceans*, 121, 5549–5569, <https://doi.org/10.1002/2015jc011542>, 2016.
- Lopes, R. and Betrouni, N.: Fractal and multifractal analysis: A review, *Medical Image Analysis*, 13, 634–649, <https://doi.org/10.1016/j.media.2009.05.003>, 2009.
- 290 Lorenz, E. N.: Deterministic Nonperiodic Flow, *Journal of the Atmospheric Sciences*, 20, 130–141, [https://doi.org/10.1175/1520-0469\(1963\)020<0130:dnf>2.0.co;2](https://doi.org/10.1175/1520-0469(1963)020<0130:dnf>2.0.co;2), 1963.



- Lucarini, V., Faranda, D., and Wouters, J.: Universal Behaviour of Extreme Value Statistics for Selected Observables of Dynamical Systems, *Journal of Statistical Physics*, 147, 63–73, <https://doi.org/10.1007/s10955-012-0468-z>, 2012.
- 295 L'Hévéder, B., Li, L., Sevault, F., and Somot, S.: Interannual variability of deep convection in the Northwestern Mediterranean simulated with a coupled AORCM, *Climate Dynamics*, 41, 937–960, <https://doi.org/10.1007/s00382-012-1527-5>, 2012.
- Madec, G. and the NEMO team: NEMO ocean engine, *Note du Pole de modelisation*, 27, 2008.
- Madec, G., Delecluse, P., Crepon, M., and Chartier, M.: A Three-Dimensional Numerical Study of Deep-Water Formation in the Northwestern Mediterranean Sea, *Journal of Physical Oceanography*, 21, 1349–1371, [https://doi.org/10.1175/1520-0485\(1991\)021<1349:atdnso>2.0.co;2](https://doi.org/10.1175/1520-0485(1991)021<1349:atdnso>2.0.co;2), 1991.
- 300 Margirier, F., Testor, P., Heslop, E., Mallil, K., Bosse, A., Houpert, L., Mortier, L., Bouin, M.-N., Coppola, L., D'Ortenzio, F., Durrieu de Madron, X., Mourre, B., Prieur, L., Raimbault, P., and Taillandier, V.: Abrupt warming and salinification of intermediate waters interplays with decline of deep convection in the Northwestern Mediterranean Sea, *Scientific Reports*, 10, <https://doi.org/10.1038/s41598-020-77859-5>, 2020.
- 305 Marshall, J. and Schott, F.: Open-ocean convection: Observations, theory, and models, *Reviews of Geophysics*, 37, 1–64, <https://doi.org/10.1029/98rg02739>, 1999.
- Robinson, A., Leslie, W., Theocharis, A., and Lascaratos, A.: *Mediterranean Sea Circulation*, p. 1689–1705, Elsevier, ISBN 9780122274305, <https://doi.org/10.1006/rwos.2001.0376>, 2001.
- Send, U. and Testor, P.: Direct Observations Reveal the Deep Circulation of the Western Mediterranean Sea, *Journal of Geophysical Research: Oceans*, 122, 10 091–10 098, <https://doi.org/10.1002/2016jc012679>, 2017.
- 310 Sérazin, G., Penduff, T., Grégorio, S., Barnier, B., Molines, J.-M., and Terray, L.: Intrinsic Variability of Sea Level from Global Ocean Simulations: Spatiotemporal Scales, *Journal of Climate*, 28, 4279–4292, <https://doi.org/10.1175/jcli-d-14-00554.1>, 2015.
- Severin, T., Kessouri, F., Rembauville, M., Sánchez-Pérez, E. D., Oriol, L., Caparros, J., Pujo-Pay, M., Ghiglione, J., D'Ortenzio, F., Taillandier, V., Mayot, N., Durrieu De Madron, X., Ulses, C., Estournel, C., and Conan, P.: Open-ocean convection process: A driver of the winter nutrient supply and the spring phytoplankton distribution in the Northwestern Mediterranean Sea, *Journal of Geophysical Research: Oceans*, 122, 4587–4601, <https://doi.org/10.1002/2016jc012664>, 2017.
- 315 Somot, S., Houpert, L., Sevault, F., Testor, P., Bosse, A., Taupier-Letage, I., Bouin, M.-N., Waldman, R., Cassou, C., Sanchez-Gomez, E., Durrieu de Madron, X., Adloff, F., Nabat, P., and Herrmann, M.: Characterizing, modelling and understanding the climate variability of the deep water formation in the North-Western Mediterranean Sea, *Climate Dynamics*, 51, 1179–1210, <https://doi.org/10.1007/s00382-016-3295-0>, 2016.
- 320 Strogatz, S. H.: *Nonlinear Dynamics And Chaos - With Applications To Physics, Biology, Chemistry, And Engineering*, Westview Press, ISBN 9780813349107, 2014.
- Testor, P. and Gascard, J.-C.: Large-Scale Spreading of Deep Waters in the Western Mediterranean Sea by Submesoscale Coherent Eddies, *Journal of Physical Oceanography*, 33, 75–87, [https://doi.org/10.1175/1520-0485\(2003\)033<0075:lssodw>2.0.co;2](https://doi.org/10.1175/1520-0485(2003)033<0075:lssodw>2.0.co;2), 2003.
- 325 Victor, J. D.: The fractal dimension of a test signal: Implications for system identification procedures, *Biological Cybernetics*, 57, 421–426, <https://doi.org/10.1007/bf00354987>, 1987.
- Waldman, R., Herrmann, M., Somot, S., Arsouze, T., Benshila, R., Bosse, A., Chanut, J., Giordani, H., Sevault, F., and Testor, P.: Impact of the Mesoscale Dynamics on Ocean Deep Convection: The 2012–2013 Case Study in the Northwestern Mediterranean Sea, *Journal of Geophysical Research: Oceans*, 122, 8813–8840, <https://doi.org/10.1002/2016jc012587>, 2017a.



- 330 Waldman, R., Somot, S., Herrmann, M., Bosse, A., Caniaux, G., Estournel, C., Houpert, L., Prieur, L., Sevault, F., and Testor, P.:  
Modeling the intense 2012-2013 dense water formation event in the northwestern Mediterranean Sea: Evaluation with an ensem-  
ble simulation approach: MODELING THE 2012-2013 DWF EVENT, *Journal of Geophysical Research: Oceans*, 122, 1297–1324,  
https://doi.org/10.1002/2016jc012437, 2017b.
- Waldman, R., Somot, S., Herrmann, M., Sevault, F., and Isachsen, P. E.: On the Chaotic Variability of Deep Convection in the Mediterranean  
335 Sea, *Geophysical Research Letters*, 45, 2433–2443, https://doi.org/10.1002/2017gl076319, 2018.